DATA, NOT MODEL: EXPLAINING BIAS TOWARD LLM TEXTS IN NEURAL RETRIEVERS

Anonymous authors
Paper under double-blind review

ABSTRACT

Recent studies show that neural retrievers often display source bias, favoring passages generated by LLMs over human-written ones, even when both are semantically similar. This bias has been considered an inherent flaw of retrievers, raising concerns about the fairness and reliability of modern information access systems. Our work challenges this view by showing that source bias stems from supervision in retrieval datasets rather than the models themselves. We found that non-semantic differences, like fluency and term specificity, exist between positive and negative documents, mirroring differences between LLM and human texts. In the embedding space, the bias direction from negatives to positives aligns with the direction from human-written to LLM-generated texts. We theoretically show that retrievers inevitably absorb the artifact imbalances in the training data during contrastive learning, which leads to their preferences over LLM texts. To mitigate the effect, we propose two approaches: 1) reducing artifact differences in training data and 2) adjusting LLM text vectors by removing their projection on the bias vector. Both methods substantially reduce source bias. We hope our study alleviates some concerns regarding LLM-generated texts in information access systems.

1 INTRODUCTION

The rapid rise of large language models (LLMs) has reshaped the information landscape, creating corpora where human-written and LLM-generated texts coexist. Within this hybrid ecosystem, an emerging phenomenon has been observed: neural retrievers often prefer LLM-generated passages over semantically similar human-written ones, a phenomenon known as source bias (Dai et al., 2024b;c). This bias raises concerns at multiple levels. For users, it risks diminishing search quality by ranking fluent but less relevant or even misleading LLM outputs above more relevant human-authored content. For human creators, it undermines fairness by systematically downranking their work and reducing its visibility. At the ecosystem level, it may amplify LLM-generated text through self-reinforcing feedback loops, further marginalizing human contributions (Chen et al., 2024; Zhou et al., 2024).

Given these significant concerns, understanding the root cause of source bias is crucial. Prior work offers different explanations: Dai et al. (2024b) attribute the bias to architectural similarities between retrievers built on pretrained language models (PLMs) and LLMs, while Wang et al. (2025) argue that retrievers prefer low-perplexity texts, a property often exhibited by LLM outputs. However, it remains unclear why such preferences emerge, and no explanation has been widely accepted. Consequently, recent efforts have shifted toward mitigating source bias, for example, through causal debiasing to reduce the impact of perplexity (Wang et al., 2025) or by aligning LLM outputs to be less biased for retrievers (Dai et al., 2025).

In this paper, we aim to uncover the root cause of source bias in neural retrievers. Specifically, we address three research questions (RQs):

- **RQ1: Is source bias a general property of neural retrievers?** Beyond the commonly studied retrievers trained on MS MARCO (Nguyen et al., 2016), we examine two additional families: (1) general-purpose embedding models trained for diverse tasks such as clustering, classification, semantic similarity, and retrieval, and (2) unsupervised retrievers trained without relevance annotations, such as Contriever (Izacard et al., 2021) and SimCSE Gao et al. (2021). We find that these models exhibit only mild source bias, whereas fine-tuning the unsupervised retrievers on MS MARCO induces severe bias. This suggests that source bias is not inherent to neural retrievers but is largely introduced through relevance supervision.

- **RQ2: Why does relevance supervision induce source bias?** Our analysis of 14 retrieval datasets uncovers systematic non-semantic differences between positive and negative documents, including variations in fluency, as measured by perplexity, and lexical specificity. These differences closely mirror the distinctions between LLM-generated and human-authored texts. In the embedding space, we further observe that the bias direction from negatives to positives aligns strongly with the direction from human-written to LLM-generated texts. Theoretical analysis confirms that retrievers trained with contrastive losses inevitably absorb these imbalances.
- **RQ3: How can source bias be mitigated?** We propose two mitigation strategies: (1) reducing artifact differences in training data to prevent retrievers from encoding non-semantic factors, and (2) debiasing embeddings by subtracting the projection of LLM-generated vectors on the bias direction. Both approaches substantially reduce source bias, confirming that it originates from systematic imbalances in relevance annotations.

In summary, we challenge the prevailing view that neural retrievers are inherently biased toward LLM-generated texts. Instead, we show that source bias arises from artifact imbalances in retrieval datasets rather than model architecture. Our findings highlight two complementary pathways for mitigation: curating training data to minimize non-semantic artifacts and explicitly decoupling artifact effects in retrievers. With a deeper understanding of source bias, LLM-generated texts need not be regarded as inherently problematic. We hope this study alleviates concerns about their use and fosters a more objective perspective on integrating LLM-generated data into retrieval systems.

2 Related Work

Source Bias in Information Retrieval. Dai et al. (2024c) revealed that neural retrievers exhibit a clear preference for LLM-generated passages even when their semantic content is similar to human-written ones, a phenomenon termed *source bias*. Cocktail (Dai et al., 2024a) further established a benchmark to evaluate this phenomenon across diverse retrieval datasets systematically. Similar effects have also been noted in related IR scenarios, including multimodal retrieval (Xu et al., 2024), recommender systems (Zhou et al., 2024), and retrieval-augmented generation (Chen et al., 2024), underscoring the view that source bias is a broad challenge in the LLM era.

Mechanisms and Mitigation. Prior work has examined both explanations and mitigations for source bias. Early studies linked it to architectural similarity between PLMs and LLMs (Dai et al., 2024c). Wang et al. (2025) showed that PLM-based retrievers overrate low-perplexity documents, and Dai et al. (2024b) framed the issue more broadly as a distribution mismatch. Mitigation approaches include retriever-side methods such as causal debiasing (Wang et al., 2025) and LLM-side methods like LLM-SBM (Dai et al., 2025). Following these perspectives, prior work has often assumed that source bias is a universal property of neural retrievers. By contrast, we evaluate a broader spectrum of retrievers and show that source bias is not inherent to neural retrievers. We further develop a retriever-centric theory and conduct a set of experiments indicating that the bias largely arises from supervision, and we provide practical mitigations.

3 RQ1: Is Source Bias a General Property of Neural Retrievers

The previously discussed phenomenon of source bias (Dai et al., 2024b;c) has been mainly observed in retrieval-supervised models, which are trained on relevance-labeled datasets such as MS MARCO (Nguyen et al., 2016). This observation prompts us to examine whether source bias is a general property of neural retrievers or a phenomenon largely induced by relevance supervision.

We therefore design two controlled experiments to disentangle the role of supervision from model architecture: (1) we examine whether source bias persists in models beyond those primarily fine-tuned on retrieval datasets, considering both general-purpose embedding models and unsupervised retrievers; and (2) we assess the impact of retrieval supervision by fine-tuning several unsupervised retrievers on MS MARCO while holding architecture fixed. Next, we present the model families, datasets, and metrics used in these experiments.

3.1 Experimental Setup

Model Families. We evaluate three distinct families of models: (A) *Relevance-Supervised Retrievers*, trained with direct or distilled supervision signals derived from large-scale human relevance annotations (e.g., MSMARCO), including ANCE(Xiong et al., 2020), TAS-B (Hofstätter et al., 2021),

Table 1: NDSR@5 results across 14 datasets for 13 neural retrievers spanning three families. Negative values (red) indicate preference for LLM-generated passages, while positive values (green) indicate preference for human-written passages.

Dataset (↓)	Relevance-Supervised Retrievers					General-Purpose Embedding Models					Unsupervised Retrievers		
	ANCE	TAS-B	coCondenser	RetroMAE	DRAGON	BGE	BCE	GTE	E5	M3E	Contriever	E5-Unsup	SimCSE
MS MARCO	-0.040	-0.119	-0.018	-0.080	-0.081	-0.021	0.084	-0.074	-0.036	0.053	0.280	0.094	0.384
DL19	-0.073	-0.224	-0.072	-0.180	-0.233	-0.017	0.119	-0.178	0.015	0.139	0.271	0.086	0.428
DL20	-0.029	-0.070	-0.078	-0.081	-0.116	0.057	0.048	-0.049	0.012	0.203	0.275	0.190	0.389
NQ	-0.040	-0.074	-0.067	-0.055	-0.096	-0.078	0.324	-0.003	0.153	0.040	0.186	0.228	0.140
NFCorpus	-0.087	-0.082	-0.067	-0.098	-0.079	0.030	-0.064	-0.142	0.034	-0.143	-0.083	-0.348	0.127
TREC-COVID	-0.162	-0.328	-0.340	-0.193	-0.133	0.014	-0.025	-0.236	-0.118	-0.085	-0.135	-0.224	0.162
HotpotQA	-0.015	-0.011	-0.008	-0.013	0.014	0.061	0.184	0.010	0.078	0.063	-0.273	-0.091	0.097
FiQA-2018	-0.179	-0.169	-0.257	-0.244	-0.160	-0.150	0.414	-0.050	-0.116	0.102	-0.068	-0.052	0.210
Touché-2020	-0.101	-0.165	-0.128	-0.099	-0.052	-0.042	0.218	-0.017	-0.185	0.242	-0.133	-0.062	0.064
DBPedia	-0.095	-0.039	-0.053	-0.077	-0.054	0.017	0.069	-0.035	0.003	0.019	-0.130	-0.062	0.064
SCIDOCS	-0.040	-0.054	-0.058	-0.073	-0.048	-0.061	0.517	-0.046	0.010	0.275	0.028	0.059	0.268
FEVER	-0.199	-0.024	-0.032	-0.006	-0.040	0.040	0.306	-0.027	0.031	0.031	0.028	-0.008	0.031
Climate-FEVER	-0.314	-0.082	-0.153	-0.105	-0.091	-0.038	0.642	-0.080	0.215	0.123	-0.003	0.017	0.070
SciFact	-0.024	-0.058	-0.049	-0.048	-0.041	0.011	0.015	-0.079	0.004	-0.206	0.017	-0.101	-0.059

coCondenser (Gao & Callan, 2021), RetroMAE (Xiao et al., 2022), and DRAGON (Lin et al., 2023); (B) *General-Purpose Embedding Models*, trained on large and diverse corpora with multi-task objectives beyond retrieval (e.g., semantic textual similarity, clustering, and classification) and widely adopted in Retrieval-Augmented Generation (RAG) applications, including BGE (Xiao et al., 2023), BCE (NetEase Youdao, 2023), GTE (Li et al., 2023), E5 (Wang et al., 2022), and M3E (Wang Yuxin, 2023); (C) *Unsupervised Retrievers*, trained without any human relevance annotations, typically via self-supervised contrastive objectives, including Contriever (Izacard et al., 2021), unsupervised SimCSE (Gao et al., 2021), and the unsupervised variant of E5 (Wang et al., 2022).

Datasets. Following recent work on source bias (Wang et al., 2025; Dai et al., 2025), We conduct experiments on the Cocktail benchmark (Dai et al., 2024a), which pairs human-written passages with LLM-generated counterparts that are semantically similar. In particular, we use the 14 datasets in Cocktail that originate from BEIR (Thakur et al., 2021), covering diverse domains such as open-domain QA, scientific retrieval, fact verification, and argumentative search. All datasets and model checkpoints are from publicly available HuggingFace releases to ensure reproducibility, with links and dataset statistics reported in Appendix B and Appendix C.

Preference Metrics. Prior work has shown that relevance-based metrics can conflate relevance with preference, and proposed the Normalized Discounted Source Ratio (NDSR) to explicitly capture source preference (Huang et al., 2025):

$$\mathrm{NDSR}_s@k = \frac{\sum_{i=1}^{k} w_i \cdot I(\mathrm{source}(d_i) = s)}{\sum_{i=1}^{k} w_i}, \quad \Delta\mathrm{NDSR}@k = \mathrm{NDSR}_{\mathrm{Human}}@k - \mathrm{NDSR}_{\mathrm{LLM}}@k,$$

where $s \in \{\mathrm{Human}, \mathrm{LLM}\}$, $I(\cdot)$ is the indicator function, $w_i = 1/\log_2(1+i)$ is a rank-based discount, and k is the cutoff. We adopt $\Delta\mathrm{NDSR}@k$ as our primary preference metric, which is bounded within $[-1, 1]$: positive values reflect preference for human-written passages, while negative values reflect preference for LLM-generated ones.

3.2 Experimental Results

Having established the model families, datasets, and evaluation metrics, we now turn to the results of our two controlled experiments. These experiments separate the influence of retrieval supervision from differences across retriever families.

Source Bias across Retriever Families. We first examine whether source bias extends beyond Relevance-Supervised Retrievers to other model families. Table 1 presents NDSR@5 results on 14 datasets for all three families. The results show that *Relevance-Supervised Retrievers* consistently favor LLM-generated passages, with negative scores on nearly all datasets, aligning with prior observations of source bias in this category. In contrast, *General-Purpose Embedding Models* and *Self-Supervised Retrievers* show no consistent pattern, with preferences varying across datasets in both directions. This suggests that source bias is not consistently present across all retriever families. In addition to these source-preference results, we also report the retrieval effectiveness of all models in Appendix D for completeness.

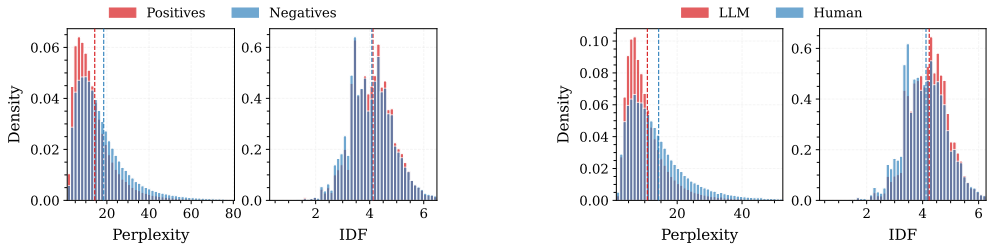

(a) Positives vs. Negatives.

(b) LLM-generated vs. Human-written.

Figure 1: Distribution of perplexity and inverse document frequency. (a) Comparison between annotated positives and the negatives in training supervision. (b) Comparison between LLM-generated and human-written passages. In both settings, the first group (Positives / LLM) exhibits lower PPL and higher IDF, revealing parallel artifact imbalances. Dashed lines indicate means.

Impact of Supervision on Source Bias. We then turn to the second experiment, where we fine-tune unsupervised retrievers on MS MARCO. In their base form (Table 1), Contriever, E5-Unsup, and SimCSE display only mild or inconsistent source preferences. After fine-tuning, however, all three models exhibit a clear shift toward favoring LLM-generated passages, as shown in Table 2. This contrast indicates that retrieval supervision is a key factor driving the observed source bias.

Summary. Taken together, these findings indicate that source bias is not an inherent property of neural retrievers but is largely induced by retrieval dataset supervision, motivating the next section on why relevance supervision gives rise to such bias.

Table 2: ΔNDSR@5 results of self-supervised retrievers after MS MARCO fine-tuning, corresponding to the same base models in Table 1. The "-FT" suffix denotes fine-tuning on MS MARCO. Negative values (red) indicate preference for LLM-generated passages, and positive values (green) indicate preference for human-written passages.

Dataset (↓)	Relevance-Supervised Retrievers		
	Contriever-FT	E5-FT	SimCSE-FT
MS MARCO	0.012	-0.044	-0.053
DL19	-0.035	-0.198	-0.133
DL20	0.121	0.022	-0.178
NQ	-0.038	-0.051	-0.060
NFCorpus	-0.139	-0.189	-0.060
TREC-COVID	-0.282	-0.271	-0.205
HotpotQA	-0.004	-0.019	-0.013
FiQA-2018	-0.215	-0.212	-0.189
Touché-2020	-0.087	-0.196	-0.169
DBPedia	-0.010	-0.036	-0.053
SCIDOCS	-0.050	-0.072	-0.041
FEVER	-0.018	-0.064	0.000
Climate-FEVER	-0.099	-0.091	-0.049
SciFact	-0.086	-0.077	-0.044

4 RQ2: Why Does Relevance Supervision Induce Source Bias?

Since source bias is largely induced by relevance supervision, we now examine why such supervision leads retrievers to prefer LLM-generated text. We hypothesize that supervised datasets introduce systematic imbalances in non-semantic artifacts between positive and negative passages, such as fluency and lexical specificity. These imbalances lead retrievers to learn to exploit these stylistic cues alongside semantic content. Positive passages in retrieval datasets are often polished and information-dense to resemble high-quality answers, a stylistic pattern that coincides with LLM-generated text. This overlap explains why retrievers tend to favor LLM-generated passages during inference. We examine this mechanism through linguistic analyses, embedding-space evidence, and a theoretical decomposition of the retrieval objective.

4.1 Linguistic Analyses

To examine whether positive passages and LLM-generated passages share similar stylistic patterns, we conduct linguistic analyses. We focus on two complementary features: perplexity (PPL), which captures fluency, and inverse document frequency (IDF), which captures lexical specificity.

Perplexity (PPL). Given a passage $d = (w_1, \ldots, w_n)$ with n tokens, its perplexity under a language model p_θ is defined as $\mathrm{PPL}(d) = \exp\left(-\frac{1}{n}\sum_{i=1}^{n}\log p_\theta(w_i \mid w_{<i})\right)$. Lower PPL corresponds to more predictable and fluent text under the model. We compute PPL using Llama-3-8B-Instruct(Dubey et al., 2024), a strong open-weight model whose training distribution offers a reliable proxy for human-perceived fluency.

Inverse Document Frequency (IDF). For a token t, its IDF is defined as $\mathrm{IDF}(t) = \log\frac{N}{1+\mathrm{df}(t)}$, where N is the total number of documents in the corpus and $\mathrm{df}(t)$ is the number of documents containing t. Passage-level IDF is computed as the median of token-level IDF values within the

passage, which provides robustness to outliers. We estimate IDF statistics on the full MS MARCO collection (∼8.8M passages), using the standard tokenizer from the Apache Lucene library Hatcher & Gospodnetic (2004) for passage segmentation.

Training Data: Positives vs. Negatives. We begin by examining the artifact imbalance between positives and negatives in training data, using MS MARCO as a representative case. Specifically, we define the positive pool as the union of passages annotated as relevant to at least one training query, and the negative pool as the remaining passages. Although the negative pool may contain unannotated false negatives, it is mostly irrelevant in practice.

Figure 1a shows that positives have lower perplexity (PPL) and a slight increase in inverse document frequency (IDF) compared to the negatives. Both differences are statistically significant; the difference in PPL is larger, while the effect of IDF is statistically reliable but small(see Appendix F for detailed statistics). Overall, positives are more fluent and marginally higher lexical specificity. This pattern is linguistically natural: annotated positives are often drawn from the main content of edited sources (e.g., news articles, Wikipedia entries, product pages), whereas the negatives covers a wider range of raw web text (e.g., forums, boilerplate, semi-structured fragments) that typically introduces disfluencies and lexically less specific patterns

Taken together, these findings show that relevance-labeled datasets exhibit artifact imbalance, as exemplified by MS MARCO. Beyond MS MARCO, we also observe consistent PPL imbalances across other IR datasets (Appendix F), suggesting that this tendency is a general property of retrieval supervision rather than an idiosyncrasy of a single dataset. This raises the question of whether similar imbalances also arise when contrasting passages by source.

Source Type: LLM-generated vs. Human-written Passages. To investigate this question, we compare LLM-generated passages with their human-written counterparts on the 14 BEIR-derived datasets from the Cocktail benchmark. For clarity of presentation, Figure 1b reports representative results on MS MARCO, where LLM-generated passages exhibit lower PPL and higher IDF than human passages, with statistically significant differences of moderate effect size(see Appendix F for detailed statistics). This pattern aligns with how LLMs are trained: pretraining on large, relatively curated corpora encourages more formal and information-dense language, yielding outputs that are more polished and lexically informative. Complete results across all 14 datasets are provided in Appendix F, with consistent patterns observed across all datasets.

Summary. Taken together, the analyses show that the artifact imbalances between positives and negatives are consistent with those between LLM-generated and human-written passages. This consistency suggests that source bias may arise from the same underlying stylistic imbalances shared between supervised datasets and LLM-generated text.

While perplexity and IDF serve as illustrative examples, they do not capture the full spectrum of stylistic artifacts. To move beyond linguistic features and connect more directly to the mechanisms of neural retrieval, we next examine how such imbalances are encoded in the embedding space.

4.2 Embedding-space Shifts

In this section, we investigate whether the embedding shift induced by supervision (positives vs. negatives) aligns with the shift induced by source type (LLM-generated vs. human-written passages). To address this, we proceed in three steps: (1) estimate the direction separating positives from negatives; (2) estimate the direction separating LLM-generated from human-written passages and assess its stability; and (3) evaluate whether the two directions are aligned.

Notation. Let $h_d(\cdot)$ denote the document encoder mapping document d to embedding $h_d(d) \in \mathbb{R}^m$, where m is the embedding dimension. $\mathbb{E}[\cdot]$ denotes expectation over specified distributions of document pairs. We use d^+ and d^- for an annotated positive and a sampled negative passage, and d_{LLM} and d_{Human} for an LLM-generated passage and its human-written counterpart. We write v for a displacement vector and $\overline{v}$ for the average displacement across pairs.

Estimating the Positive–Negative Embedding Direction. To estimate an embedding direction that primarily reflects stylistic artifacts rather than semantic variation, it is important to ensure that the positive and negative pools have comparable semantic distributions. In MS MARCO, however, positives and negatives differ systematically in topical coverage. Following common practice in

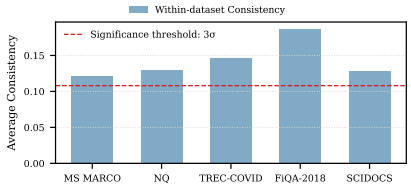

(a) Within-dataset consistency.

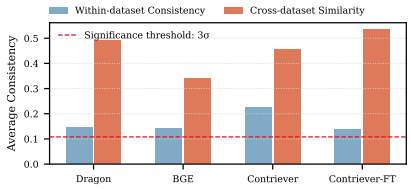

(c) Cross-retriever consistency.

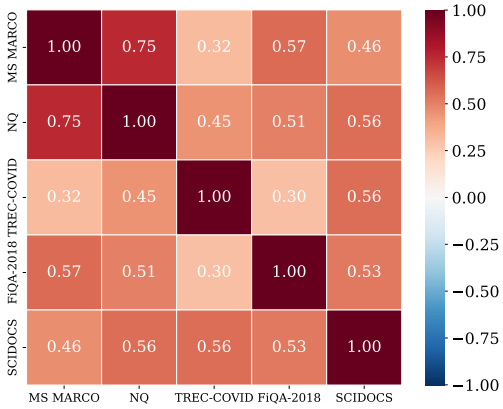

(b) Cross-dataset consistency.

Figure 2: The LLM–Human distinction forms a stable embedding-space direction. The plots demonstrate this consistency along three dimensions: (a) within datasets, (b) across datasets, and (c) across retrievers. All metrics shown exceeded the 3σ threshold. Plots (a, b) use the DRAGON retriever; results for all 14 datasets are in Appendix H.

(Karpukhin et al., 2020), we mitigate this by retrieving the top-10 BM25 candidates for each query and randomly sampling one as the negative, yielding a 1:1 pairing with the annotated positive. This construction balances topical distributions, allowing the mean embedding contrast between positives and negatives to more accurately isolate non-semantic artifacts. Formally, we estimate the supervision-induced embedding direction as $\overline{v}_{\text{p-n}} = \mathbb{E}\big[h_d(d^+) - h_d(d^-)\big]$.

Significance Criterion in High-Dimensional Space. Before turning to the LLM–Human direction, we first establish a statistical threshold to test whether displacement vectors exhibit a coherent direction rather than random noise. In 768 dimensions, random vectors are almost orthogonal, with cosine similarities concentrated around zero. Over 99.7% of random pairs fall within $\pm 3\sigma$ of the mean (Appendix G). Deviations beyond this range therefore indicate a consistent, non-random effect. We use this as the significance criterion for subsequent analyses.

Is the LLM–Human Distinction a Stable Embedding Direction? Unlike the positive–negative setting, the LLM–Human comparison is constructed with semantically aligned counterparts, which allows us to directly compute the displacement. We then examine whether the displacement $\Delta v(d) = h_d(d_{\text{LLM}}) - h_d(d_{\text{Human}})$ forms a coherent embedding-space direction along three dimensions: (1) *Within datasets*, we test whether the average pairwise cosine similarity among displacement vectors, $\mathbb{E}_{i \neq j}[\cos(\Delta v(d_i), \Delta v(d_j))]$, exceeds the significance threshold, indicating coherent rather than random shifts (Figure 2a). (2) *Across datasets*, we compute dataset-level mean displacements $\overline{\Delta v}_{\text{dataset}} = \mathbb{E}_{d \in \text{dataset}}[\Delta v(d)]$ and assess whether they are aligned (i.e., $\cos(\overline{\Delta v}_{D_1}, \overline{\Delta v}_{D_2})$), indicating a shared direction across datasets (Figure 2b). (3) *Across models*, this consistency is observed both within and across datasets, and it holds robustly across all retrievers examined (Figure 2c). Taken together, the results demonstrate that the LLM–human distinction corresponds to a stable embedding-space direction rather than noise specific to individual datasets or models.

Do the Positive–Negative and LLM–Human Directions Align? Having established that the LLM–human distinction corresponds to a stable embedding direction, we now test our central hypothesis: whether this direction aligns with the supervision-induced positive–negative direction, $\overline{v}_{\text{p-n}}$. We measure this alignment by computing the cosine similarity between the mean LLM–human direction for each dataset, $\overline{\Delta v}_{\text{dataset}}$, and the positive–negative direction derived from MS MARCO. As shown in Figure 3a, the alignment is consistently strong and statistically significant across all datasets. Furthermore, this effect is not specific to a single retriever. Figure 3b shows that the alignment remains robustly significant across retrievers. This strong, consistent alignment demonstrates that the positive-negative and LLM-human distinctions correspond to a shared direction in the embedding space. We now turn to our theoretical framework to formalize the mechanism by which this alignment emerges as a learnable shortcut for relevance, thus inducing source bias.

4.3 THEORETICAL FRAMEWORK: ARTIFACT ENCODING IN NEURAL RETRIEVERS

Building on the linguistic and embedding-space analyses, we formalize these observations in a theoretical framework. For clarity and intuition, this section presents an informal overview of our key results (see Appendix E for formal statements and proofs). Our theory shows that (1) whenever training data contains systematic artifact imbalances, the retriever necessarily learns these non-semantic cues, and (2) these cues manifest as an approximately linear component in the retrieval score.

To illustrate this, we abstractly decompose any document d into its semantic features M_d and its non-semantic artifact features A_d (e.g., fluency, lexical patterns). An *artifact imbalance* exists if positive passages systematically differ from negative passages in their artifact features. Specifically, we define the artifact imbalance at training time as the difference between the expected artifact features of positive and negative documents: $\Delta_A = \mathbb{E}[A_{d^+}] - \mathbb{E}[A_{d^-}]$. Here A_{d^+} and A_{d^-} represent the artifact features of positive and negative documents, respectively.

Our first key result is that such imbalance directly shapes the optimal retriever's scoring function.

Proposition 1 (Decomposition of the Optimal Scorer, Informal)**.** *The Bayes-optimal retrieval score $s^*(\cdot,\cdot)$, which is approximated by models trained with contrastive objectives like InfoNCE, necessarily decomposes into a semantic term and an artifact-dependent term:*

$$s^*(q,d) = \mathrm{Score}_{\mathrm{semantic}}(q, M_d) + \mathrm{Score}_{\mathrm{artifact}}(q, A_d).$$

If the training data exhibit artifact imbalance ($\Delta_A \neq 0$), the artifact-dependent term is non-zero.

> **Insight 1:** Artifact imbalance forces the optimal retriever to encode non-semantic cues. The model learns that artifacts like high fluency are predictive of relevance, creating a shortcut.

Next, we connect this decomposition to the practical implementation of dot-product retrievers.

Proposition 2 (Embedding-Space Decomposition, Informal)**.** *For a standard dot-product retriever, the retrieval score $s_\theta(\cdot,\cdot)$ can be approximated as a sum of a semantic and an artifact-based score:*

$$s_\theta(q,d) \;=\; \langle h_q(q), h_d(d)\rangle \;\approx\; \underbrace{\langle h_q(q),\, h_d^{\mathrm{sem}}(d)\rangle}_{\textit{semantic}} \;+\; \underbrace{\langle h_q(q),\, h_d^{\mathrm{art}}(d)\rangle}_{\textit{artifact}}.$$

This decomposition can be viewed as a first-order Taylor approximation. The document encoder, though a complex non-linear model, can be locally approximated as linear in the artifact features, which is consistent with our empirical observation of a stable direction in embedding space.

> **Insight 2:** The artifact-based score is captured by a linear operation in the embedding space.

Why Other Families Do Not Exhibit Consistent Source Bias. Unlike relevance-supervised retrievers, other retriever families do not exhibit a consistent source bias. (1) General-purpose embedding models are trained on diverse tasks such as semantic textual similarity, natural language inference, clustering, and classification. Many of these objectives are symmetric: if sentence a is a positive for sentence b, then b is a positive for a. Such symmetry prevents systematic differences between "positives" and "negatives," yielding $\Delta_A \approx 0$ and avoiding artifact-driven shortcuts. (2) Unsupervised retrievers like Contriever rely on self-supervised objectives constructed directly from raw corpora, where adjacent spans of text are treated as positives and other in-batch samples serve as negatives. Because no annotated positive–negative splits are involved, the training signal lacks systematic stylistic imbalance. In both cases, the artifact-dependent term in Proposition 1 averages out in expectation, explaining why these models do not exhibit a consistent source bias (Section 3).

Summary. Our analyses consistently show that source bias arises from artifact imbalance in training data. Linguistically, positives in supervision and LLM-generated passages both show lower perplexity and increased lexical specificity than their counterparts. In embedding space, the supervision-induced positive–negative direction and the LLM–human displacement align as a stable, shared axis. Our theoretical framework formalizes this observation: any artifact imbalance in training necessarily introduces a linear artifact component into the retriever's scoring function. This explains why stylistic imbalances observed in supervision manifest as a stable embedding direction spuriously aligned with relevance, providing both a mechanistic account of source bias and a foundation for mitigation strategies.

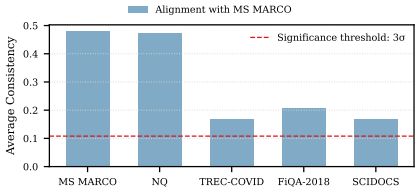

(a) Cross-dataset consistency.

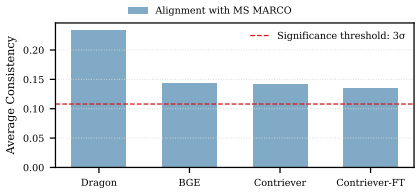

(b) Cross-retriever consistency.

Figure 4: The LLM–human direction aligns with the positive–negative supervision direction. This alignment is consistent across datasets (a) and across different retrievers (b), with all results being statistically significant.

Table 3: ΔNDSR@5 results under different negative sampling strategies. "In-batch only" suppresses artifact imbalance ($\Delta_A \approx 0$), "Standard" combines in-batch and hard negatives, and "Hard-neg only" maximizes artifact imbalance.

	In-batch only	Standard	Hard-neg only
MS MARCO	0.014	-0.051	-0.057
DL19	0.025	-0.155	-0.182
DL20	0.041	-0.120	-0.152
NQ	0.020	-0.081	-0.085
NFCorpus	-0.050	-0.068	-0.093
TREC-COVID	-0.182	-0.252	-0.285
HotpotQA	0.003	0.017	-0.021
FiQA-2018	-0.055	-0.227	-0.238
Touché-2020	-0.077	-0.202	-0.193
DBPedia	-0.021	-0.041	-0.043
SCIDOCS	0.010	-0.051	-0.035
FEVER	0.014	-0.005	-0.013
Climate-FEVER	-0.032	-0.071	-0.080
SciFact	-0.032	-0.051	-0.053
AVG	-0.024	-0.099	-0.109

Table 4: ΔNDSR@5 results (original vs. debias) across 5 datasets for 5 relevance-supervised retrievers. Positive values indicate preference for human-written passages, negative values indicate preference for LLM-generated passages. Full results on 14 datasets are provided in Appendix I.

Dataset (↓)	ANCE		coCondenser		DRAGON		RetroMAE		TAS-B	
	Original	Debias	Original	Debias	Original	Debias	Original	Debias	Original	Debias
MS MARCO	-0.042	0.168	-0.020	0.094	-0.083	-0.065	-0.083	0.011	-0.121	-0.062
TREC-COVID	-0.162	-0.178	-0.340	-0.281	-0.134	-0.154	-0.194	-0.098	-0.328	-0.248
NQ	-0.042	-0.032	-0.072	-0.071	-0.099	-0.085	-0.060	-0.044	-0.078	-0.062
FiQA-2018	-0.179	-0.159	-0.219	-0.263	-0.161	-0.154	-0.205	-0.201	-0.170	-0.182
SCIDOCS	-0.040	0.069	-0.058	-0.053	-0.048	-0.012	-0.073	0.007	-0.054	0.010
AVG	-0.093	-0.026	-0.142	-0.115	-0.105	-0.094	-0.123	-0.072	-0.150	-0.109

5 RQ3: How can source bias be mitigated?

Building on our theoretical results, we now move from explanation to mechanism validation and bias mitigation. Proposition 1 revealed that artifact imbalance ($\Delta_A \neq 0$) in supervision necessarily leads the retriever to encode non-semantic cues, while Proposition 2 showed that these cues manifest as a linear component in embedding space. These insights suggest two complementary strategies: reduce Δ_A during training or suppress the artifact direction at inference. Importantly, these interventions not only mitigate source bias but also validate its underlying mechanism: if reducing Δ_A or removing the artifact direction reliably diminishes bias, this provides strong empirical support for our theoretical account. In summary, our aim is not to advance state-of-the-art debiasing, but to substantiate the mechanism of source bias and propose simple interventions that are readily applicable in practice. We therefore examine both strategies below.

Training-time Interventions: Controlling Artifact Imbalance (Δ_A). We propose a simple training-time mitigation strategy: adopting *in-batch only* negative sampling, where negatives are exclusively other queries' positives from the annotated pool. This setup ensures $\mathbb{E}[A_{d^+}] \approx \mathbb{E}[A_{d^-}]$ and thus suppresses artifact imbalance ($\Delta_A \approx 0$). To evaluate its effectiveness, we contrast it against two reference settings: (1) the *standard* sampling scheme widely used for training neural retrievers, which combines in-batch negatives with one mined hard negative per query and yields a moderate Δ_A; and (2) a *hard-neg only* setting, which draws negatives solely from the unannotated pool and maximizes Δ_A. Together, these three conditions provide a controlled spectrum of artifact imbalance.

Table 5: NDCG@5 results (original vs. debias) on 5 datasets for 5 relevance-supervised retrievers. Full results on 14 datasets are provided in Appendix I.

Dataset (↓)	ANCE		coCondenser		DRAGON		RetroMAE		TAS-B	
	Original	Debias	Original	Debias	Original	Debias	Original	Debias	Original	Debias
MS MARCO	0.590	0.568	0.620	0.621	0.665	0.665	0.626	0.626	0.617	0.617
TREC-COVID	0.679	0.690	0.707	0.695	0.684	0.681	0.744	0.737	0.644	0.638
NQ	0.628	0.626	0.687	0.687	0.737	0.737	0.704	0.704	0.689	0.689
FiQA-2018	0.255	0.255	0.244	0.244	0.323	0.322	0.278	0.277	0.257	0.261
SCIDOCS	0.114	0.113	0.124	0.125	0.148	0.146	0.136	0.136	0.138	0.133
AVG	0.453	0.450	0.477	0.474	0.511	0.510	0.497	0.496	0.468	0.467

For fairness and controllability, we fine-tune BERT-based retrievers on MSMARCO using the official BEIR pipeline(Devlin et al., 2019; Thakur et al., 2021), modifying only the negative sampling strategy while keeping all other factors fixed. This isolates the impact of sampling on source bias.

As shown in Table 3, the in-batch only strategy substantially reduces source bias, improving the average ΔNDSR@5 from -0.099 (standard sampling) to -0.024, whereas standard and hard-neg only sampling lead to progressively stronger bias. Although omitting mined hard negatives slightly impairs retrieval effectiveness (average NDCG@5 drops from 0.493 to 0.475, see Appendix I), the reduction in bias is considerable. These findings validate our theoretical account and demonstrate that mitigation at training time is indeed effective, providing a useful pivot for further exploration of debiasing strategies. Building on this, we next examine inference-time interventions that suppress artifact directions without retraining.

Inference-time Interventions: Suppressing Artifact Directions. Our analyses in Section 4.2 showed that LLM-generated passages induce a consistent displacement in embedding space.Let $n = \frac{\overline{\Delta v}}{\|\overline{\Delta v}\|}$ denote the normalized mean displacement between LLM rewrites and their human counterparts. In practice, we estimate n by averaging displacement vectors from 1000 randomly sampled human–LLM passage pairs per dataset. This sampling size yields stable estimates across datasets while remaining computationally efficient. At inference, for passage embedding $v \in \mathbb{R}^m$, we suppress the component along n: $v' = v - (v \cdot n)\, n$.

We focus on five relevance-supervised retrievers, where source bias is most pronounced and our theoretical analysis directly applies. As shown in Tables 4 and 5, the projection reduces source bias in most cases, while retrieval effectiveness is largely preserved. Importantly, it requires no retraining and adds negligible computational cost, as embeddings are already computed during inference. This provides a practical drop-in solution that can be readily integrated into existing retrieval systems.

Summary. These interventions jointly achieve mechanism validation and mitigation. Training-time sampling strategies directly manipulate Δ_A, showing a consistent trend where larger imbalance leads to stronger bias, thereby establishing a clear link between supervision artifacts and source bias. Inference-time projection complements this by suppressing artifact-driven directions in embedding space, reducing bias with negligible cost and no retraining. Together, these complementary approaches both reinforce our theoretical account and provide practical strategies for mitigating source bias in deployed retrieval systems.

6 CONCLUSION

This paper re-examines the origins of source bias in neural retrieval and shows that it is not an inherent property but a learned consequence of artifact imbalance in supervised training data. Through theoretical analysis and empirical validation, we demonstrate how contrastive objectives encode non-semantic artifacts and how LLM-generated text mirrors these artifacts, producing a consistent biased direction in embedding space. Building on this insight, we introduce two mitigation methods: (1) a training-time negative sampling control that effectively mitigates source bias, and (2) an inference-time projection that achieves similar debiasing strength while largely preserving retrieval performance. Our findings indicate that artifact imbalance is an important factor behind source bias, motivating the development of de-artifacted datasets and training practices for more robust and fair retrieval systems. More broadly, the analyses and mitigation strategies explored here may inform the study of other spurious correlations across domains.

REFERENCES

Alexander Bondarenko, Maik Fröbe, Meriem Beloucif, Lukas Gienapp, Yamen Ajjour, Alexander Panchenko, Chris Biemann, Benno Stein, Henning Wachsmuth, Martin Potthast, et al. Overview of touché 2020: argument retrieval. In *International Conference of the Cross-Language Evaluation Forum for European Languages*, pp. 384–395. Springer, 2020.

Vera Boteva, Demian Gholipour, Artem Sokolov, and Stefan Riezler. A full-text learning to rank dataset for medical information retrieval. In *European Conference on Information Retrieval*, pp. 716–722. Springer, 2016.

Xiaoyang Chen, Ben He, Hongyu Lin, Xianpei Han, Tianshu Wang, Boxi Cao, Le Sun, and Yingfei Sun. Spiral of silence: How is large language model killing information retrieval?–a case study on open domain question answering. *arXiv preprint arXiv:2404.10496*, 2024.

Arman Cohan, Sergey Feldman, Iz Beltagy, Doug Downey, and Daniel S Weld. Specter: Document-level representation learning using citation-informed transformers. *arXiv preprint arXiv:2004.07180*, 2020.

Nick Craswell, Bhaskar Mitra, Emine Yilmaz, Daniel Campos, and Ellen M. Voorhees. Overview of the trec 2019 deep learning track, 2020. URL https://arxiv.org/abs/2003.07820.

Nick Craswell, Bhaskar Mitra, Emine Yilmaz, and Daniel Campos. Overview of the trec 2020 deep learning track, 2021. URL https://arxiv.org/abs/2102.07662.

Sunhao Dai, Weihao Liu, Yuqi Zhou, Liang Pang, Rongju Ruan, Gang Wang, Zhenhua Dong, Jun Xu, and Ji-Rong Wen. Cocktail: A comprehensive information retrieval benchmark with llm-generated documents integration. *arXiv preprint arXiv:2405.16546*, 2024a.

Sunhao Dai, Chen Xu, Shicheng Xu, Liang Pang, Zhenhua Dong, and Jun Xu. Bias and unfairness in information retrieval systems: New challenges in the llm era. In *Proceedings of the 30th ACM SIGKDD Conference on Knowledge Discovery and Data Mining*, pp. 6437–6447, 2024b.

Sunhao Dai, Yuqi Zhou, Liang Pang, Weihao Liu, Xiaolin Hu, Yong Liu, Xiao Zhang, Gang Wang, and Jun Xu. Neural retrievers are biased towards llm-generated content. In *Proceedings of the 30th ACM SIGKDD Conference on Knowledge Discovery and Data Mining*, pp. 526–537, 2024c.

Sunhao Dai, Yuqi Zhou, Liang Pang, Zhuoyang Li, Zhaocheng Du, Gang Wang, and Jun Xu. Mitigating source bias with llm alignment. In *Proceedings of the 48th International ACM SIGIR Conference on Research and Development in Information Retrieval*, pp. 370–380, 2025.

Jacob Devlin, Ming-Wei Chang, Kenton Lee, and Kristina Toutanova. Bert: Pre-training of deep bidirectional transformers for language understanding. In *Proceedings of the 2019 conference of the North American chapter of the association for computational linguistics: human language technologies, volume 1 (long and short papers)*, pp. 4171–4186, 2019.

Thomas Diggelmann, Jordan Boyd-Graber, Jannis Bulian, Massimiliano Ciaramita, and Markus Leippold. Climate-fever: A dataset for verification of real-world climate claims. *arXiv preprint arXiv:2012.00614*, 2020.

Abhimanyu Dubey, Abhinav Jauhri, Abhinav Pandey, Abhishek Kadian, Ahmad Al-Dahle, Aiesha Letman, Akhil Mathur, Alan Schelten, Amy Yang, Angela Fan, et al. The llama 3 herd of models. *arXiv preprint arXiv:2407.21783*, 2024.

Luyu Gao and Jamie Callan. Unsupervised corpus aware language model pre-training for dense passage retrieval. *arXiv preprint arXiv:2108.05540*, 2021.

Tianyu Gao, Xingcheng Yao, and Danqi Chen. Simcse: Simple contrastive learning of sentence embeddings. *arXiv preprint arXiv:2104.08821*, 2021.

Faegheh Hasibi, Fedor Nikolaev, Chenyan Xiong, Krisztian Balog, Svein Erik Bratsberg, Alexander Kotov, and Jamie Callan. Dbpedia-entity v2: a test collection for entity search. In *Proceedings of the 40th international ACM SIGIR conference on research and development in information retrieval*, pp. 1265–1268, 2017.

Erik Hatcher and Otis Gospodnetic. *Lucene in action (in action series)*. Manning Publications Co., 2004.

Sebastian Hofstätter, Sheng-Chieh Lin, Jheng-Hong Yang, Jimmy Lin, and Allan Hanbury. Efficiently teaching an effective dense retriever with balanced topic aware sampling. In *Proceedings of the 44th international ACM SIGIR conference on research and development in information retrieval*, pp. 113–122, 2021.

Wei Huang, Keping Bi, Yinqiong Cai, Wei Chen, Jiafeng Guo, and Xueqi Cheng. How do llm-generated texts impact term-based retrieval models? *arXiv preprint arXiv:2508.17715*, 2025.

Gautier Izacard, Mathilde Caron, Lucas Hosseini, Sebastian Riedel, Piotr Bojanowski, Armand Joulin, and Edouard Grave. Unsupervised dense information retrieval with contrastive learning. *arXiv preprint arXiv:2112.09118*, 2021.

Vladimir Karpukhin, Barlas Oguz, Sewon Min, Patrick SH Lewis, Ledell Wu, Sergey Edunov, Danqi Chen, and Wen-tau Yih. Dense passage retrieval for open-domain question answering. In *EMNLP (1)*, pp. 6769–6781, 2020.

Tom Kwiatkowski, Jennimaria Palomaki, Olivia Redfield, Michael Collins, Ankur Parikh, Chris Alberti, Danielle Epstein, Illia Polosukhin, Jacob Devlin, Kenton Lee, et al. Natural questions: a benchmark for question answering research. *Transactions of the Association for Computational Linguistics*, 7:453–466, 2019.

Zehan Li, Xin Zhang, Yanzhao Zhang, Dingkun Long, Pengjun Xie, and Meishan Zhang. Towards general text embeddings with multi-stage contrastive learning. *arXiv preprint arXiv:2308.03281*, 2023.

Sheng-Chieh Lin, Akari Asai, Minghan Li, Barlas Oguz, Jimmy Lin, Yashar Mehdad, Wen-tau Yih, and Xilun Chen. How to train your dragon: Diverse augmentation towards generalizable dense retrieval. *arXiv preprint arXiv:2302.07452*, 2023.

Macedo Maia, Siegfried Handschuh, André Freitas, Brian Davis, Ross McDermott, Manel Zarrouk, and Alexandra Balahur. Www'18 open challenge: financial opinion mining and question answering. In *Companion proceedings of the the web conference 2018*, pp. 1941–1942, 2018.

Inc. NetEase Youdao. Bcembedding: Bilingual and crosslingual embedding for rag. `https://github.com/netease-youdao/BCEmbedding`, 2023.

Tri Nguyen, Mir Rosenberg, Xia Song, Jianfeng Gao, Saurabh Tiwary, Rangan Majumder, and Li Deng. MS MARCO: A human generated machine reading comprehension dataset. In Tarek Richard Besold, Antoine Bordes, Artur S. d'Avila Garcez, and Greg Wayne (eds.), *Proceedings of the Workshop on Cognitive Computation: Integrating neural and symbolic approaches 2016 co-located with the 30th Annual Conference on Neural Information Processing Systems (NIPS 2016), Barcelona, Spain, December 9, 2016*, volume 1773 of *CEUR Workshop Proceedings*. CEUR-WS.org, 2016. URL `https://ceur-ws.org/Vol-1773/CoCoNIPS_2016_paper9.pdf`.

Nandan Thakur, Nils Reimers, Andreas Rücklé, Abhishek Srivastava, and Iryna Gurevych. Beir: A heterogenous benchmark for zero-shot evaluation of information retrieval models. *arXiv preprint arXiv:2104.08663*, 2021.

James Thorne, Andreas Vlachos, Christos Christodoulopoulos, and Arpit Mittal. Fever: a large-scale dataset for fact extraction and verification. *arXiv preprint arXiv:1803.05355*, 2018.

Roman Vershynin. *High-dimensional probability: An introduction with applications in data science*, volume 47. Cambridge university press, 2018.

Ellen Voorhees, Tasmeer Alam, Steven Bedrick, Dina Demner-Fushman, William R Hersh, Kyle Lo, Kirk Roberts, Ian Soboroff, and Lucy Lu Wang. Trec-covid: constructing a pandemic information retrieval test collection. In *ACM SIGIR Forum*, volume 54, pp. 1–12. ACM New York, NY, USA, 2021.

David Wadden, Shanchuan Lin, Kyle Lo, Lucy Lu Wang, Madeleine van Zuylen, Arman Cohan, and Hannaneh Hajishirzi. Fact or fiction: Verifying scientific claims. *arXiv preprint arXiv:2004.14974*, 2020.

Haoyu Wang, Sunhao Dai, Haiyuan Zhao, Liang Pang, Xiao Zhang, Gang Wang, Zhenhua Dong, Jun Xu, and Ji-Rong Wen. Perplexity trap: Plm-based retrievers overrate low perplexity documents. *arXiv preprint arXiv:2503.08684*, 2025.

Liang Wang, Nan Yang, Xiaolong Huang, Binxing Jiao, Linjun Yang, Daxin Jiang, Rangan Majumder, and Furu Wei. Text embeddings by weakly-supervised contrastive pre-training. *arXiv preprint arXiv:2212.03533*, 2022.

He sicheng Wang Yuxin, Sun Qingxuan. M3e: Moka massive mixed embedding model, 2023.

Shitao Xiao, Zheng Liu, Yingxia Shao, and Zhao Cao. Retromae: Pre-training retrieval-oriented language models via masked auto-encoder. *arXiv preprint arXiv:2205.12035*, 2022.

Shitao Xiao, Zheng Liu, Peitian Zhang, and Niklas Muennighoff. C-pack: Packaged resources to advance general chinese embedding, 2023.

Lee Xiong, Chenyan Xiong, Ye Li, Kwok-Fung Tang, Jialin Liu, Paul Bennett, Junaid Ahmed, and Arnold Overwijk. Approximate nearest neighbor negative contrastive learning for dense text retrieval. *arXiv preprint arXiv:2007.00808*, 2020.

Shicheng Xu, Danyang Hou, Liang Pang, Jingcheng Deng, Jun Xu, Huawei Shen, and Xueqi Cheng. Ai-generated images introduce invisible relevance bias to text-image retrieval. In *ICLR 2024 Workshop on Reliable and Responsible Foundation Models*, 2024.

Zhilin Yang, Peng Qi, Saizheng Zhang, Yoshua Bengio, William W Cohen, Ruslan Salakhutdinov, and Christopher D Manning. Hotpotqa: A dataset for diverse, explainable multi-hop question answering. *arXiv preprint arXiv:1809.09600*, 2018.

Yuqi Zhou, Sunhao Dai, Liang Pang, Gang Wang, Zhenhua Dong, Jun Xu, and Ji-Rong Wen. Source echo chamber: Exploring the escalation of source bias in user, data, and recommender system feedback loop. *CoRR*, 2024.

A The Use of Large Language Models (LLMs)

In this study, we employed Large Language Models (LLMs) as an AI writing assistant, using them strictly to improve the clarity and readability of our textual expressions. The models were not used for research ideation, literature retrieval, or discovery, nor to generate any substantive suggestions.

B Reproducibility Resources

To ensure reproducibility, we provide the full list of datasets and model checkpoints used in this work. All datasets and models are obtained from publicly available HuggingFace releases or their official websites. Our usage strictly follows the respective licenses and research-only terms of the original sources. Tables 6 and 7 provide direct links for reference.

C Dataset Statistics

Table 8 summarizes the statistics of the 14 datasets used in this paper. This table is adapted from the Cocktail benchmark (Dai et al., 2024a), with minor modifications.

D Retrieval Effectiveness of Evaluated Models

For completeness, we report the retrieval effectiveness of all evaluated models on the Cocktail benchmark. Table 9 presents NDCG@5 across 14 datasets for the 13 retrievers spanning the three model families. Table 10 further reports results after fine-tuning self-supervised retrievers on MS MARCO. These results complement the source preference analyses in Section 3.

Table 6: Datasets used in this paper (Cocktail versions) and their HuggingFace links.

Dataset	HuggingFace Link
MS MARCO (Nguyen et al., 2016)	https://huggingface.co/datasets/IR-Cocktail/msmarco
TREC-DL'19 (Craswell et al., 2020)	https://huggingface.co/datasets/IR-Cocktail/dl19
TREC-DL'20 (Craswell et al., 2021)	https://huggingface.co/datasets/IR-Cocktail/dl20
Natural Questions (Kwiatkowski et al., 2019)	https://huggingface.co/datasets/IR-Cocktail/nq
NFCorpus (Boteva et al., 2016)	https://huggingface.co/datasets/IR-Cocktail/nfcorpus
TREC-COVID (Voorhees et al., 2021)	https://huggingface.co/datasets/IR-Cocktail/trec-covid
HotpotQA (Yang et al., 2018)	https://huggingface.co/datasets/IR-Cocktail/hotpotqa
FiQA-2018 (Maia et al., 2018)	https://huggingface.co/datasets/IR-Cocktail/fiqa
Touché-2020 (Bondarenko et al., 2020)	https://huggingface.co/datasets/IR-Cocktail/webis-touche2020
DBpedia-Entity (Hasibi et al., 2017)	https://huggingface.co/datasets/IR-Cocktail/dbpedia-entity
SciDocs (Cohan et al., 2020)	https://huggingface.co/datasets/IR-Cocktail/scidocs
FEVER (Thorne et al., 2018)	https://huggingface.co/datasets/IR-Cocktail/fever
Climate-FEVER (Diggelmann et al., 2020)	https://huggingface.co/datasets/IR-Cocktail/climate-fever
SciFact (Wadden et al., 2020)	https://huggingface.co/datasets/IR-Cocktail/scifact

Table 7: Dense retriever checkpoints used in this paper and their HuggingFace links.

Model	HuggingFace Link
Relevance-Supervised Retrievers	
ANCE (Xiong et al., 2020)	https://huggingface.co/sentence-transformers/msmarco-roberta-base-ance-firstp
TAS-B (Hofstätter et al., 2021)	https://huggingface.co/sentence-transformers/msmarco-distilbert-base-tas-b
coCondenser (Gao & Callan, 2021)	https://huggingface.co/sentence-transformers/msmarco-bert-co-condensor
RetroMAE (Xiao et al., 2022)	https://huggingface.co/nthakur/RetroMAE_BEIR
DRAGON (query encoder) (Lin et al., 2023)	https://huggingface.co/nthakur/dragon-plus-query-encoder
DRAGON (corpus encoder) (Lin et al., 2023)	https://huggingface.co/nthakur/dragon-plus-context-encoder
General-Purpose Embedding Models	
BGE-base (Xiao et al., 2023)	https://huggingface.co/BAAI/bge-base-en-v1.5
BCE (NetEase Youdao, 2023)	https://huggingface.co/maidalun1020/bce-embedding-base_v1
GTE (Li et al., 2023)	https://huggingface.co/thenlper/gte-base
E5 (Wang et al., 2022)	https://huggingface.co/intfloat/e5-base-v2
M3E (Wang Yuxin, 2023)	https://huggingface.co/moka-ai/m3e-base
Self-Supervised Retrievers	
Contriever (Izacard et al., 2021)	https://huggingface.co/nishimoto/contriever-sentencetransformer
E5-Unsupervised (Wang et al., 2022)	https://huggingface.co/intfloat/e5-base-unsupervised
SimCSE (Gao et al., 2021)	https://huggingface.co/princeton-nlp/unsup-simcse-bert-base-uncased

E Formal Statements and Proofs

We formalize the intuition that artifact imbalance biases retrieval by analyzing how it affects the retriever's learning objective in three steps: (1) derive the Bayes-optimal retrieval scorer, (2) decompose it into semantic and artifact terms, and (3) relate this decomposition to an embedding-space view that bridges theory with practical retriever representations.

Notation and Setting. Let q denote a query and d a document. Each document d is associated with semantic features M_d and artifact features A_d (e.g., perplexity, IDF profile, stylistic attributes), both treated as random vectors. We consider dense retrievers consisting of a dual-encoder and a scoring function. The dual-encoder maps queries and documents into embeddings $h_q(q), h_d(d) \in \mathbb{R}^m$, and a typical scoring function is the inner product $s_\theta(q,d) = \langle h_q(q), h_d(d) \rangle$.

Training relies on positive and negative query–document pairs. Let $p_{\text{pos}}(q,d)$ denote the distribution of positive pairs, and let $p(q)p(d)$ be the reference distribution given by independent sampling of queries and documents. Positives (q, d^+) are drawn from $p_{\text{pos}}(q,d)$, while negatives (q, d^-) are sampled from $p(q)p(d)$—a standard abstraction of in-batch and hard-negative schemes. We define the *artifact imbalance* at training time as $\Delta_A = \mathbb{E}[A_{d^+}] - \mathbb{E}[A_{d^-}]$.

Step 1: Optimal scorer under InfoNCE. InfoNCE is a widely used contrastive learning objective, which encourages the retriever to assign higher scores to positive pairs (q, d^+) than to negatives (q, d^-), thereby pulling queries closer to their relevant documents while pushing them away from irrelevant ones. The Bayes-optimal retriever is therefore given by the following lemma.

Lemma 1. *For contrastive learning with negatives sampled independently from $p(d)$, the Bayes-optimal scorer of a dense retriever is $s^*(q,d) = \log \frac{p_{\text{pos}}(q,d)}{p(q)p(d)} + C$, where C is an additive constant that does not depend on d.*

Insight 1: Retriever training with InfoNCE is equivalent to estimating a log-density ratio.

Step 2: Decomposition into semantic and artifact terms. Building on this formulation, we view each document as consisting of semantic features M_d and artifact features A_d, under which the density-ratio admits the following decomposition.

Table 8: Statistics of the 14 datasets in the Cocktail benchmark used in this paper. Avg. D/Q denotes the average number of relevant documents per query. This table is adapted from Dai et al. (2024a).

Dataset	Domain	Task	Relevancy	#Pairs	#Queries	#Corpus	Avg. D/Q	Avg. Length (Q / Human / LLM)
MS MARCO	Misc.	Passage Retrieval	Binary	532,663	6,979	542,203	1.1	6.0 / 58.1 / 55.1
DL19	Misc.	Passage Retrieval	Binary	-	43	542,203	95.4	5.4 / 58.1 / 55.1
DL20	Misc.	Passage Retrieval	Binary	-	54	542,203	66.8	6.0 / 58.1 / 55.1
TREC-COVID	Biomedical	Biomedical IR	3-level	-	50	128,585	430.1	10.6 / 197.6 / 165.9
NFCorpus	Biomedical	Biomedical IR	3-level	110,575	323	3,633	38.2	3.3 / 221.0 / 206.7
NQ	Wikipedia	QA	Binary	-	3,446	104,194	1.2	9.2 / 86.9 / 81.0
HotpotQA	Wikipedia	QA	Binary	169,963	7,405	111,107	2.0	17.7 / 67.9 / 66.6
FiQA-2018	Finance	QA	Binary	14,045	648	57,450	2.6	10.8 / 133.2 / 107.8
Touché-2020	Misc.	Argument Retrieval	3-level	-	49	101,922	18.4	6.6 / 165.4 / 134.4
DBPedia	Wikipedia	Entity Retrieval	3-level	-	400	145,037	37.3	5.4 / 53.1 / 54.0
SCIDOCS	Scientific	Citation Prediction	Binary	-	1,000	25,259	4.7	9.4 / 169.7 / 161.8
FEVER	Wikipedia	Fact Checking	Binary	140,079	6,666	114,529	1.2	8.1 / 113.4 / 91.1
Climate-FEVER	Wikipedia	Fact Checking	Binary	-	1,535	101,339	3.0	20.2 / 99.4 / 81.3
SciFact	Scientific	Fact Checking	Binary	919	300	5,183	1.1	12.4 / 201.8 / 192.7

Table 9: NDCG@5 results across 14 datasets for 13 dense retrievers. Higher is better.

Dataset (↓)	Relevance-Supervised Retrievers					General-Purpose Embedding Models					Self-Supervised Retrievers		
	ANCE	TAS-B	coCondenser	RetroMAE	DRAGON	BGE	BCE	GTE	E5	M3E	Contriever	E5-Unsup	SimCSE
MS MARCO	0.647	0.680	0.683	0.688	0.735	0.688	0.590	0.688	0.702	0.473	0.504	0.575	0.245
DL19	0.686	0.760	0.734	0.743	0.771	0.755	0.708	0.750	0.747	0.507	0.515	0.624	0.346
DL20	0.701	0.724	0.708	0.751	0.758	0.729	0.651	0.718	0.743	0.489	0.492	0.597	0.289
NQ	0.640	0.708	0.711	0.746	0.790	0.778	0.625	0.789	0.790	0.494	0.623	0.737	0.353
NFCorpus	0.266	0.340	0.345	0.336	0.389	0.403	0.275	0.394	0.368	0.257	0.339	0.371	0.109
TREC-COVID	0.671	0.670	0.677	0.735	0.678	0.783	0.574	0.763	0.714	0.390	0.391	0.605	0.296
HotpotQA	0.553	0.705	0.663	0.747	0.799	0.792	0.533	0.761	0.801	0.575	0.650	0.668	0.369
FiQA-2018	0.275	0.408	0.467	0.498	0.529	0.384	0.285	0.380	0.373	0.366	0.225	0.373	0.093
Touché-2020	0.479	0.427	0.349	0.441	0.390	0.402	0.333	0.423	0.411	0.242	0.308	0.333	0.252
DBPedia	0.408	0.493	0.493	0.528	0.533	0.514	0.360	0.514	0.541	0.370	0.427	0.488	0.259
SCIDOCS	0.095	0.111	0.102	0.116	0.123	0.177	0.118	0.190	0.141	0.069	0.114	0.174	0.041
FEVER	0.820	0.835	0.842	0.870	0.876	0.928	0.682	0.924	0.905	0.865	0.878	0.925	0.510
Climate-FEVER	0.270	0.306	0.255	0.311	0.318	0.368	0.274	0.373	0.303	0.161	0.223	0.264	0.195
SciFact	0.465	0.602	0.549	0.611	0.631	0.715	0.533	0.732	0.688	0.448	0.614	0.719	0.239

Proposition 3. *Let $T(d) = (M_d, A_d)$ be a measurable mapping decomposing a document into semantic and artifact features. Then* $\log \frac{p_{\mathrm{pos}}(q,d)}{p(q)p(d)} = \underbrace{\phi(q, M_d)}_{\textit{semantic}} + \underbrace{\psi\big(A_d \,\big|\, q, M_d\big)}_{\textit{artifact}}$. *If the training sampler induces artifact imbalance (e.g., $\Delta_A \neq 0$), then the Bayes-optimal scorer necessarily carries an artifact-dependent term. In particular, $I(s^*(q,d); A_d \mid q, M_d) > 0$.*

> **Insight 2:** Whenever artifact imbalance exists, the Bayes-optimal scorer necessarily carries an artifact-dependent term.

Step 3: An idealized embedding-space view. To translate the above decomposition into an embedding-space view, we focus on the dot-product retriever. Under a linear approximation, its score decomposes into two inner products, explicitly separating semantic and artifact contributions.

Proposition 4. *For a dot-product retriever with query encoder h_q and passage encoder h_d, suppose each passage d can be abstractly decomposed into semantic features M_d and artifact features A_d. Then, under a linear approximation,* $s_\theta(q,d) = \underbrace{\langle h_q(q),\, h_{\mathrm{sem}}(M_d)\rangle}_{\textit{semantic}} + \underbrace{\langle h_q(q),\, h_{\mathrm{art}}(A_d)\rangle}_{\textit{artifact (linear)}}$, *where $h_{\mathrm{sem}}(M_d)$ and $h_{\mathrm{art}}(A_d)$ denote the semantic and artifact representations, respectively.*

> **Insight 3:** Under a linear approximation, the retriever's score explicitly decomposes into semantic and artifact contributions in the embedding space.

Formal proofs of Lemma 1, Proposition 3, and Proposition 4 are provided in Appendix E.1. Together, these results specify the conditions under which supervision can induce source bias: when training data exhibit artifact imbalance, the optimal scorer encodes artifact-dependent signals alongside semantic content. The analysis further predicts that such artifacts correspond to linearly decodable directions in the embedding space, offering a concrete signature for empirical validation. This perspective clarifies when and how source bias may emerge and provides testable predictions that motivate the empirical analyses that follow.

Table 10: NDCG@5 results of self-supervised retrievers after MS MARCO fine-tuning, corresponding to the same base models in Table 9. The "-FT" suffix denotes fine-tuning on MS MARCO.

Dataset (↓)	Relevance-Supervised Retrievers		
	Contriever-FT	E5-FT	SimCSE-FT
MS MARCO	0.676	0.711	0.630
DL19	0.696	0.763	0.727
DL20	0.673	0.720	0.703
NQ	0.732	0.764	0.670
NFCorpus	0.339	0.378	0.279
TREC-COVID	0.446	0.731	0.590
HotpotQA	0.712	0.735	0.577
FiQA-2018	0.255	0.336	0.220
Touché-2020	0.347	0.428	0.389
DBPedia	0.495	0.532	0.444
SCIDOCS	0.117	0.138	0.083
FEVER	0.857	0.895	0.837
Climate-FEVER	0.289	0.312	0.261
SciFact	0.593	0.679	0.470

E.1 Proof of Lemma 1

This appendix provides the formal proofs of the main theoretical results presented in Section 4.3. Specifically, we include detailed proofs of Lemma 1, Proposition 3, and Proposition 4.

Proof. We derive the Bayes-optimal scorer for InfoNCE under independent negative sampling. The proof proceeds in three steps: (i) formalize the sampling and objective, (ii) show that risk minimization forces the predictor to match the true posterior, and (iii) compute this posterior and simplify.

Step 1: Sampling scheme and objective. Draw a query $q \sim p(q)$ and sample an index $I \sim \mathrm{Unif}\{0, \dots, K\}$ to determine the position of the positive passage. Conditioned on (q, I), sample $d_I \sim p_{\mathrm{pos}}(d \mid q)$ and $d_j \sim p(d)$ for $j \neq I$, giving $\boldsymbol{d} = (d_0, \dots, d_K)$.

Given scores $s(q, d_j) \in \mathbb{R}$, the model predicts

$$\pi_\theta(i \mid q, \boldsymbol{d}) = \frac{\exp\big(s(q, d_i)\big)}{\sum_{j=0}^{K} \exp\big(s(q, d_j)\big)}. \tag{1}$$

In practice, a temperature parameter τ is often included (i.e., $s(q, d) = \langle h_q(q), h_d(d) \rangle / \tau$). We omit τ for notational simplicity, as it only rescales the scores.

The InfoNCE loss is the expected negative log-likelihood (cross-entropy):

$$\mathcal{L}(\theta) = \mathbb{E}_{(q,\boldsymbol{d})}\Big[\, \mathbb{E}_{I|q,\boldsymbol{d}}\big[-\log \pi_\theta(I \mid q, \boldsymbol{d})\big] \,\Big] = \mathbb{E}_{(q,\boldsymbol{d})}\big[R(\boldsymbol{s}; q, \boldsymbol{d})\big], \tag{2}$$

where we denote $P_i = \mathbb{P}(I = i \mid q, \boldsymbol{d})$ and $\pi_i = \pi_\theta(i \mid q, \boldsymbol{d})$

$$R(\boldsymbol{s}; q, \boldsymbol{d}) = -\sum_{i=0}^{K} P_i \log \pi_i. \tag{3}$$

Step 2: Bayes optimality. This risk decomposes as

$$R(\boldsymbol{s}; q, \boldsymbol{d}) = -\sum_{i=0}^{K} P_i \log \pi_i = \underbrace{\big(-\sum_i P_i \log P_i\big)}_{H(P)} + \sum_i P_i \log \frac{P_i}{\pi_i} \;=\; H(P) + \mathrm{KL}(P \| \pi). \tag{4}$$

Since $H(P)$ is independent of θ and $\mathrm{KL}(P\|\pi) \geq 0$ with equality iff $\pi = P$, we have

$$\pi_\theta(\cdot \mid q, \boldsymbol{d}) \text{ minimizes } R(\boldsymbol{s}; q, \boldsymbol{d}) \quad \Longleftrightarrow \quad \pi_\theta(\cdot \mid q, \boldsymbol{d}) = P(\cdot \mid q, \boldsymbol{d}). \tag{5}$$

Because $\pi_\theta(i \mid q, \boldsymbol{d}) = \frac{\exp(s(q,d_i))}{\sum_j \exp(s(q,d_j))}$ is a softmax over scores, any optimizer must satisfy

$$s(q, d_i) = \log P_i \;+\; C(q, \boldsymbol{d}), \tag{6}$$

for some additive constant $C(q, \boldsymbol{d})$ that is shared across all i (hence irrelevant to the softmax).

Step 3: Compute the posterior. To compute P_i, note that by Bayes' rule and the sampling scheme,

$$P_i = \mathbb{P}(I = i \mid q, \boldsymbol{d}) \propto \mathbb{P}(I = i)\, p(q)\, p(d_i \mid I = i, q) \prod_{j \neq i} p(d_j \mid I = i, q) \tag{7}$$

$$= \frac{1}{K+1}\, p(q)\, p_{\mathrm{pos}}(d_i \mid q) \prod_{j \neq i} p(d_j), \tag{8}$$

where we used $p(d_j \mid I = i, q) = p(d_j)$ for $j \neq i$ and $p(d_i \mid I = i, q) = p_{\mathrm{pos}}(d_i \mid q)$. Normalizing over i yields

$$\mathbb{P}(I = i \mid q, \boldsymbol{d}) = \frac{\dfrac{p_{\mathrm{pos}}(d_i \mid q)}{p(d_i)}}{\displaystyle\sum_{j=0}^{K} \frac{p_{\mathrm{pos}}(d_j \mid q)}{p(d_j)}}. \tag{9}$$

Taking logs and plugging into the optimality condition above, we obtain

$$s^*(q, d_i) = \log P_i + C(q, \boldsymbol{d}) \tag{10}$$

$$= \log \frac{p_{\mathrm{pos}}(d_i \mid q)}{p(d_i)} - \log \left(\sum_{j=0}^{K} \frac{p_{\mathrm{pos}}(d_j \mid q)}{p(d_j)} \right) + C(q, \boldsymbol{d}) \tag{11}$$

$$= \log \frac{p_{\mathrm{pos}}(q, d)}{p(q)\, p(d)} + \log p(q) - \log p_{\mathrm{pos}}(q) - \log \left(\sum_{j=0}^{K} \frac{p_{\mathrm{pos}}(d_j \mid q)}{p(d_j)} \right) + C(q, \boldsymbol{d}) \tag{12}$$

The last four terms are independent of d (they depend only on q or the batch $\boldsymbol{d}$). Since the softmax is invariant to adding any constant shared across candidates, they can be absorbed into a single additive constant. Hence the Bayes-optimal scorer is equivalently

$$s^*(q, d) = \log \frac{p_{\mathrm{pos}}(q, d)}{p(q)\, p(d)} + C, \tag{13}$$

for some constant C that does not depend on d. This completes the proof.

Remark. If negatives are drawn from a distribution $p_{\mathrm{neg}}(d)$ other than $p(d)$, the same derivation yields $s^*(q, d) = \log \frac{p_{\mathrm{pos}}(d|q)}{p_{\mathrm{neg}}(d)} + C$. In all cases, s^* is unique up to adding any function of q. □

E.2 Proof of Proposition 3

Proof. The goal is to show that the density ratio naturally decomposes into a semantic term and an artifact term; if the artifact distribution differs between positives and negatives, the artifact contribution cannot vanish.

We use uppercase letters (e.g., M_d, A_d) to denote random vectors, and lowercase m, a for their realizations. The argument proceeds by a change of variables. If T is further assumed to be C^1 and bijective onto its image, then

$$p_{\mathrm{pos}}(q, m, a) = p_{\mathrm{pos}}(q, d)\, |\det J_T(d)|^{-1}, \tag{14}$$

$$p(m, a) = p(d)\, |\det J_T(d)|^{-1}. \tag{15}$$

Thus,

$$\frac{p_{\mathrm{pos}}(q, d)}{p(q)p(d)} = \frac{p_{\mathrm{pos}}(q, m, a)}{p(q)p(m, a)}. \tag{16}$$

Applying the chain rule twice gives

$$\log \frac{p_{\mathrm{pos}}(q, m, a)}{p(q)\, p(m, a)} = \big[\log p_{\mathrm{pos}}(q \mid m, a) - \log p(q) \big] + \big[\log p_{\mathrm{pos}}(m, a) - \log p(m, a) \big]. \tag{17}$$

Decompose further as $\log p_{\text{pos}}(m, a) = \log p_{\text{pos}}(m) + \log p_{\text{pos}}(a \mid m)$ and $\log p(m, a) = \log p(m) + \log p(a \mid m)$, and add–subtract $\log p_{\text{pos}}(q \mid m)$ to isolate the (q, m) contribution:

$$\log \frac{p_{\text{pos}}(q, m, a)}{p(q)\, p(m, a)} = \underbrace{\big[\log p_{\text{pos}}(q \mid m) - \log p(q)\big] + \big[\log p_{\text{pos}}(m) - \log p(m)\big]}_{\phi(q,m)} + \underbrace{\big[\log p_{\text{pos}}(q \mid m, a) - \log p_{\text{pos}}(q \mid m)\big] + \big[\log p_{\text{pos}}(a \mid m) - \log p(a \mid m)\big]}_{\psi(a|q,m)}. \tag{18}$$

If $p_{\text{pos}}(a \mid q, m) \neq p(a \mid m)$ on a set of positive measure, then the artifact term ψ cannot vanish. Since $s^*(q, d) = \phi(q, m) + \psi(a \mid q, m) + C$ is a deterministic function of (q, m, a), we have

$$H(s^* \mid q, m, a) = 0. \tag{19}$$

If $A \mid (q, m)$ is non-degenerate and $\psi(\cdot \mid q, m)$ is non-constant, then the distribution of s^* given (q, m) is non-degenerate, i.e.

$$H(s^* \mid q, m) > 0. \tag{20}$$

Consequently,

$$I(A; s^* \mid q, m) = H(s^* \mid q, m) - H(s^* \mid q, m, a) > 0, \tag{21}$$

which establishes the claim. □

E.3 Proof of Proposition 4

Proof. Let $T : \mathcal{D} \to \mathcal{M} \times \mathcal{A}$ be a C^1 bijection onto its image with $T(d) = (M_d, A_d)$, and let the passage encoder $h_d : \mathcal{D} \to \mathbb{R}^m$ be C^1. Define $g(m, a) \coloneqq h_d(T^{-1}(m, a))$ and fix a reference $a_0 \in \mathcal{A}$. Then for (m, a) near (m, a_0),

$$g(m, a) \;=\; g(m, a_0) \;+\; J_a(m, a_0)\,(a - a_0) \;+\; r(m, a), \quad \|r(m, a)\| = o(\|a - a_0\|),$$

where $J_a(m, a_0) = \big[\partial g(m, a)/\partial a\big]_{a=a_0}$. Writing

$$h_{\text{sem}}(m) \coloneqq g(m, a_0), \qquad h_{\text{art}}(a;\, m) \coloneqq J_a(m, a_0)\,(a - a_0),$$

we obtain the local additive form

$$h_d(d) \;=\; h_{\text{sem}}(M_d) \;+\; h_{\text{art}}(A_d;\, M_d) \;+\; r(M_d, A_d).$$

At this point, we make a simplifying assumption: the Jacobian $J_a(m, a_0)$ does not substantially depend on m, or any residual dependence can be absorbed into the remainder term. Under this idealization we may write $h_{\text{art}}(a;\, m) \approx h_{\text{art}}(a)$.

Consequently, for a dot-product retriever $s_\theta(q, d) = \langle h_q(q), h_d(d) \rangle$,

$$s_\theta(q, d) \;=\; \underbrace{\langle h_q(q), h_{\text{sem}}(M_d) \rangle}_{\text{semantic}} \;+\; \underbrace{\langle h_q(q), h_{\text{art}}(A_d) \rangle}_{\text{artifact (linear)}} \;+\; \varepsilon(q, M_d, A_d), \tag{22}$$

where $\varepsilon(q, M_d, A_d) \coloneqq \langle h_q(q), r(M_d, A_d) \rangle$ satisfies $\varepsilon(q, M_d, A_d) = o(\|A_d - a_0\|)$ as $\|A_d - a_0\| \to 0$. In other words, the remainder vanishes to first order and can be neglected in the idealized decomposition. □

Remark. The argument relies on a local first-order approximation and a simplifying assumption on the artifact Jacobian. These approximations are introduced only to obtain a clearer analytical decomposition of semantic and artifact contributions. In the main text, we empirically examine whether artifact features can be linearly decodable from $h_d(d)$, providing evidence in support of this idealized view.

F Additional Linguistic Analyses

In this appendix, we provide supplementary analyses promised in Section 4.1. Specifically, we report (i) additional effect-size analyses for the comparisons in the main text, and (ii) results on the other 13 datasets beyond MS MARCO.

F.1 Effect-Size Analyses

We quantify the magnitude of linguistic differences using standard effect-size measures (Hedges' g for mean differences) and report associated significance levels. These statistics complement the significance tests in the main paper by showing not only whether differences are significant but also their practical magnitude. Table 11 summarizes results on MS MARCO for two contrasts: (i) positives vs. the unannotated pool, and (ii) LLM-generated vs. human-written passages.

Table 11: Effect sizes (Hedges' g) and significance for linguistic feature comparisons on MS MARCO. Positive values indicate higher scores for the first group. p-values smaller than numerical precision are reported as $p < 10^{-15}$.

Comparison	PPL (g)	IDF (g)	p-value
Positives vs. Unannotated	-0.214	$+0.047$	$< 10^{-15}$
LLM vs. Human	-0.274	$+0.145$	$< 10^{-15}$

We observe that both comparisons yield highly significant differences despite modest effect sizes. For perplexity (PPL), positives are more fluent than the unannotated pool ($g = -0.214$), and LLM passages are even more fluent than human passages ($g = -0.274$). For IDF, the effects are smaller ($g = 0.047$ and 0.145 respectively) but consistently positive, indicating that both positives and LLM rewrites exhibit slightly greater lexical specificity. Taken together, these results show that supervision and source type both introduce systematic, statistically robust shifts in linguistic features, even if the magnitudes are moderate.

F.2 Positives vs. Negatives on Additional Datasets

To assess whether the imbalance between annotated positives and negatives generalizes beyond MSMARCO, we extend the perplexity analysis to other datasets in Cocktail (Figure5). For datasets that share the same corpus (e.g., MSMARCO and DL19/20), we report results only once. For NFCorpus and HotpotQA, all passages are annotated with relevance labels, so no negative pool exists and only positives are shown. Across the remaining datasets, positives consistently exhibit lower perplexity than negatives, mirroring the trend in MSMARCO. This indicates that stylistic disparities between positives and negatives are not dataset-specific idiosyncrasies but a systematic property of retrieval supervision. As discussed in the main text, positives are often drawn from edited, high-quality sources intended to serve as good answers, whereas negatives derive from more heterogeneous and less polished text.

F.3 LLM vs. Human across Additional Datasets

To ensure that the findings generalize beyond MS MARCO, we replicate the analysis on the other datasets in Cocktail. Figure 6 reports perplexity distributions, and Figure 7 reports IDF distributions, comparing LLM-generated versus human-written passages.

Consistent with the MS MARCO case, LLM-generated passages consistently exhibit lower perplexity and slightly higher IDF than their human-written counterparts. The PPL differences are stable and clear across all datasets, while the IDF differences are more modest in magnitude but follow the same direction throughout. These results confirm that source-based stylistic artifacts are systematic and broadly consistent across domains.

G Cosine Similarity Between Random High-Dimensional Vectors

We derive the null distribution of cosine similarities between independent random vectors, which serves as the statistical baseline for our embedding-space analyses. Let $x, y \in \mathbb{R}^d$ be isotropic random vectors. Normalizing to the unit sphere ($\hat{x} = x/\|x\|, \hat{y} = y/\|y\|$) yields $\hat{x}, \hat{y} \sim \mathrm{Unif}(\mathbb{S}^{d-1})$, and their cosine similarity is

$$Z = \langle \hat{x}, \hat{y} \rangle \in [-1, 1].$$

By rotational invariance, Z follows a Beta-type density (Vershynin, 2018):

$$f_Z(z) \;=\; \frac{\Gamma(\frac{d}{2})}{\sqrt{\pi}\,\Gamma(\frac{d-1}{2})}(1-z^2)^{\frac{d-3}{2}}, \quad z \in [-1, 1],$$

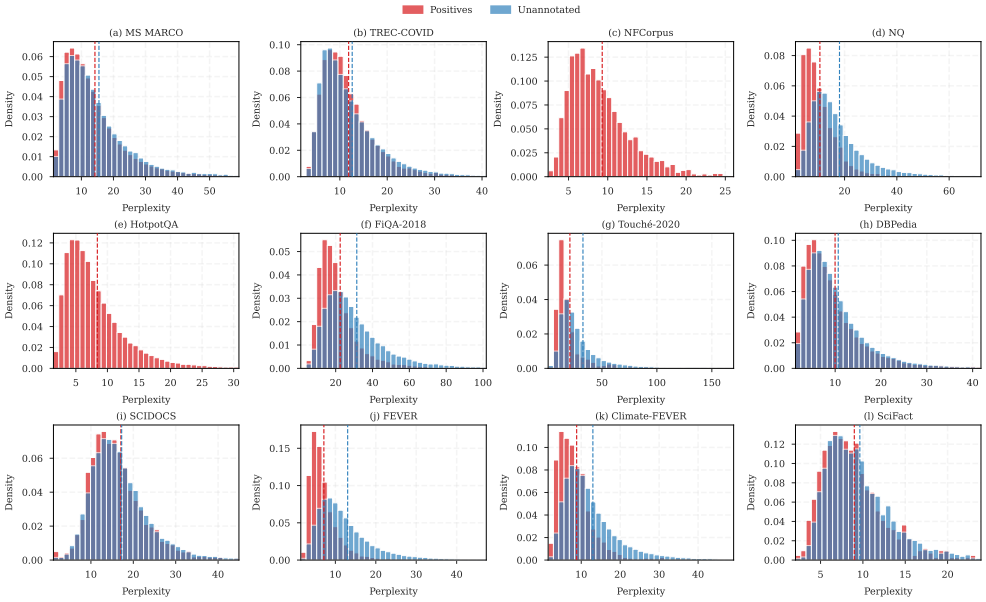

Figure 5: Perplexity distributions of positives versus negatives across retrieval datasets in Cocktail. For MS MARCO and DL19/20, results are reported once due to corpus overlap. For NFCorpus and HotpotQA, all passages are annotated as relevant, so only positive distributions are shown.

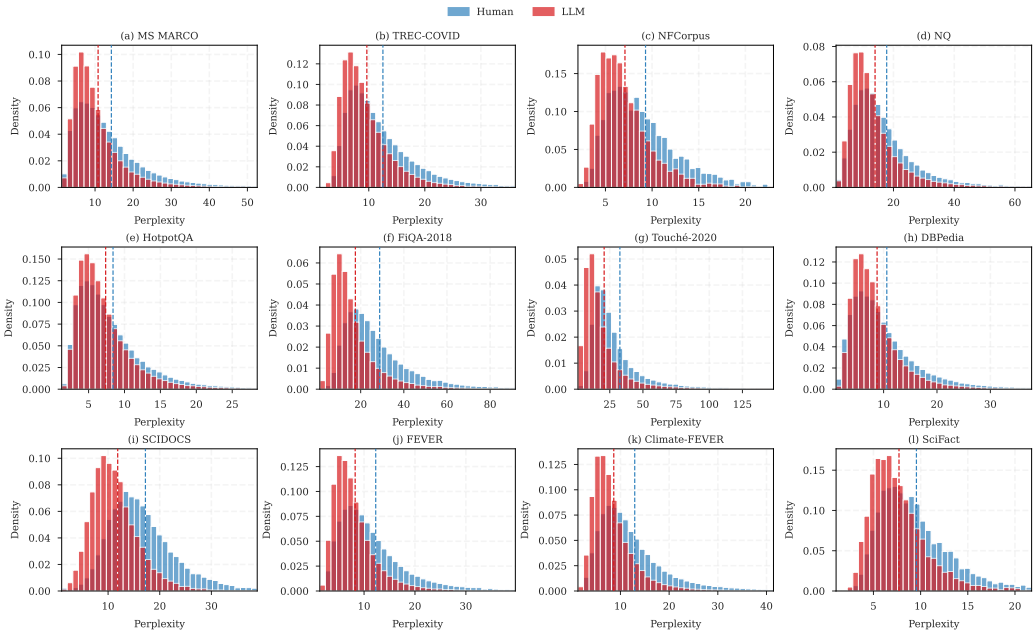

Figure 6: Perplexity (PPL) distributions of LLM-generated vs. human-written passages across additional datasets. Red = LLM, Blue = Human. LLM passages consistently exhibit lower perplexity, indicating higher fluency.

which is symmetric around zero. Equivalently, the tail probability can be expressed via the regularized incomplete Beta function:

$$\Pr(|Z| > t) \;=\; \mathrm{I}_{1-t^2}\!\left(\tfrac{d-1}{2},\, \tfrac{1}{2}\right).$$

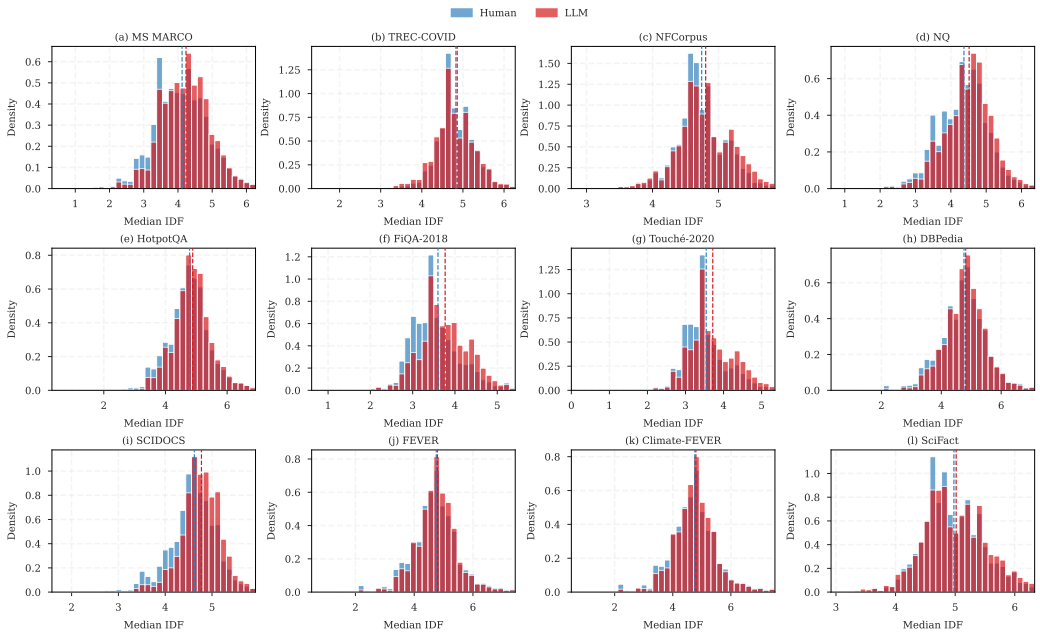

Figure 7: Median IDF distributions of LLM-generated vs. human-written passages across additional datasets. Red = LLM, Blue = Human. LLM passages generally exhibit higher IDF, though the gap varies across datasets.

By symmetry, $\mathbb{E}[Z] = 0$. Since each coordinate of a uniform unit vector has variance $1/d$, the variance of Z is

$$\mathrm{Var}(Z) = \frac{1}{d}.$$

For large d, the density concentrates sharply at zero. Expanding $\log(1 - z^2) \approx -z^2$ near the origin gives the Gaussian approximation

$$Z \approx \mathcal{N}\big(0, \tfrac{1}{d}\big).$$

In dimension $d = 768$, the standard deviation is $\sigma = 1/\sqrt{d} \approx 0.0361$, so that $3\sigma \approx 0.108$. Under the normal approximation,

$$\Pr(|Z| > 3\sigma) \approx 0.27\%,$$

which closely matches the exact Beta distribution. Thus, over 99.7% of random pairs fall within $\pm 3\sigma$, validating the use of this threshold as a significance criterion in high-dimensional embedding spaces. Figure 8 illustrates this concentration.

H Additional Embedding Analyses

In this appendix, we provide the full embedding-space analyses across all 12 distinct corpora in the Cocktail benchmark, using the Dragon retriever as a representative model. Our experiments use 14 datasets from the Cocktail benchmark. Since three of them (MS MARCO, DL19, and DL20) share the same underlying corpus, we report embedding statistics at the corpus level, resulting in 12 unique corpora. These figures complement the representative results shown in the main text and report: (1) within-dataset displacement consistency (Figure 9), (2) cross-dataset similarity of mean displacement directions (Figure 10), and (3) alignment between LLM–human and supervision-induced directions (Figure 11).

Overall, these results extend the main-text findings to the full set of datasets. The majority of datasets follow the same trends as reported in the main text, while a small number exhibit weaker effects, which we discuss as exceptions rather than contradictions.

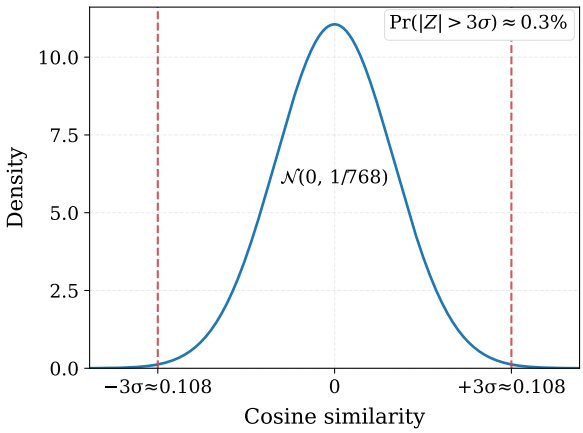

Figure 8: Null distribution of cosine similarity between random vectors in $d = 768$ dimensions, approximated by $\mathcal{N}(0, 1/d)$. Over 99.7% of values lie within $\pm 3\sigma \approx 0.108$, supporting its use as a significance criterion.

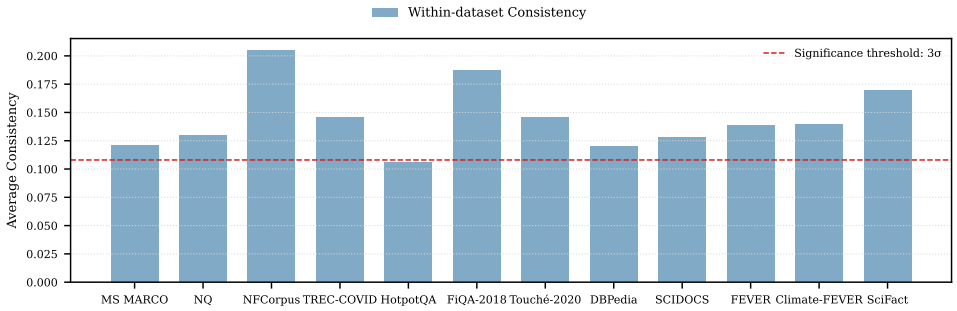

Figure 9: Within-dataset consistency of LLM–human displacements. Bars show average pairwise cosine similarity among displacement vectors $\Delta v(d)$ within each dataset, relative to the 3σ significance threshold. Most datasets exceed the threshold, with a few exceptions near or below it.

I Additional Results for RQ3

In this section, we provide the supplementary results for Section 5, including (a) retrieval effectiveness for the training-time sampling experiments, which were omitted from the main text due to space constraints, and (b) additional inference-time debiasing results on more datasets. These results complement the main findings and further validate our conclusions.

I.1 Training-time Interventions: Retrieval Effectiveness

Table 12 reports retrieval effectiveness (NDCG@5) for the three negative sampling strategies (*in-batch only*, *standard*, and *hard-neg only*) across all datasets. Overall, settings that include mined hard negatives achieve higher retrieval performance, while using only in-batch negatives leads to lower effectiveness on most datasets. This trend is consistent with widely noted observations in the dense retrieval community that mined hard negatives are essential for strong retrieval effectiveness.

I.2 Inference-time Interventions: Additional Datasets

We extend the inference-time evaluation beyond the five datasets shown in the main text. Table 13 reports NDSR@5 across all datasets, while Table 14 shows the corresponding NDCG@5 results. Overall, the projection method generally reduces source bias, while retrieval effectiveness is largely preserved across datasets, consistent with the main text findings.

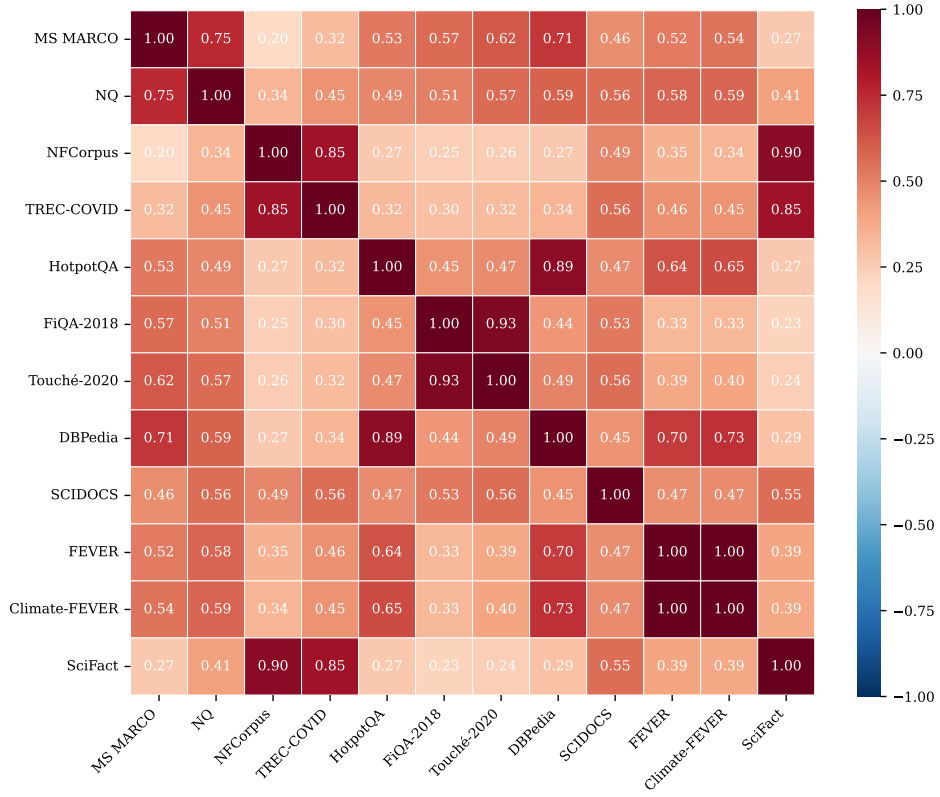

Figure 10: Cross-dataset similarity of mean LLM–human displacement directions. Values denote cosine similarity between dataset-level means $\overline{\Delta v}$. Darker cells indicate stronger alignment, revealing consistent artifact-induced directions across corpora.

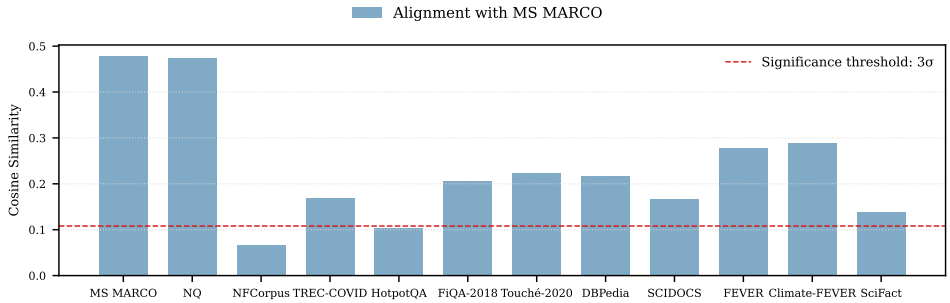

Figure 11: Cosine similarity between the LLM–human displacement direction and the MS MARCO positive–negative contrast, across datasets. The red dashed line marks the 3σ significance threshold derived under the random null. Most datasets show strong alignment beyond the threshold, with a few cases near or below it.

Table 12: NDCG@5 results on 14 datasets under different negative sampling strategies. The "Standard" strategy combines in-batch and hard negatives, while the other two use only one type.

Dataset	In-batch only	Standard	Hard-neg only
MS MARCO	0.629	0.629	0.623
DL19	0.640	0.706	0.728
DL20	0.642	0.701	0.719
TREC-COVID	0.571	0.611	0.568
NFCorpus	0.303	0.287	0.278
NQ	0.652	0.670	0.666
HotpotQA	0.570	0.579	0.579
FiQA-2018	0.209	0.218	0.216
Touché-2020	0.350	0.418	0.411
DBPedia	0.428	0.436	0.437
SCIDOCS	0.096	0.086	0.086
FEVER	0.850	0.842	0.829
Climate-FEVER	0.280	0.271	0.241
SciFact	0.435	0.452	0.443
AVG	0.475	0.493	0.487

Table 13: NDSR@5 results (original vs. debias) across 5 datasets for 5 relevance-supervised retrievers. Positive values indicate preference for human-written passages, negative values indicate preference for LLM-generated passages.

Dataset (↓)	ANCE		coCondenser		DRAGON		RetroMAE		TAS-B	
	Original	Debias	Original	Debias	Original	Debias	Original	Debias	Original	Debias
MS MARCO	-0.042	0.168	-0.020	0.094	-0.083	-0.065	-0.083	0.011	-0.121	-0.062
DL19	-0.073	0.197	-0.072	0.096	-0.233	-0.160	-0.186	0.076	-0.224	-0.151
DL20	-0.034	0.270	-0.079	0.011	-0.121	-0.103	-0.088	0.015	-0.072	0.007
TREC-COVID	-0.162	-0.178	-0.340	-0.281	-0.134	-0.154	-0.194	-0.098	-0.328	-0.248
NFCorpus	-0.087	-0.067	-0.068	-0.064	-0.079	-0.064	-0.081	-0.044	-0.082	-0.057
NQ	-0.042	-0.032	-0.072	-0.071	-0.099	-0.085	-0.060	-0.044	-0.078	-0.062
HotpotQA	-0.020	0.014	-0.014	0.029	-0.018	-0.031	-0.019	0.045	-0.018	-0.024
FiQA-2018	-0.179	-0.159	-0.219	-0.263	-0.161	-0.154	-0.205	-0.201	-0.170	-0.182
Touché-2020	-0.168	-0.148	-0.226	-0.153	-0.178	-0.162	-0.175	-0.127	-0.247	-0.197
DBPedia	-0.097	0.025	-0.054	-0.015	-0.057	-0.055	-0.059	0.006	-0.042	-0.036
SCIDOCS	-0.040	0.069	-0.058	-0.053	-0.048	-0.012	-0.073	0.007	-0.054	0.010
FEVER	-0.200	-0.061	-0.037	-0.041	-0.043	-0.031	-0.010	0.031	-0.029	-0.029
Climate-FEVER	-0.314	-0.225	-0.153	-0.066	-0.091	-0.066	-0.105	0.023	-0.083	-0.064
SciFact	-0.025	-0.020	-0.049	-0.033	-0.041	-0.042	-0.048	-0.043	-0.058	-0.063
AVG	-0.106	-0.011	-0.104	-0.036	-0.099	-0.084	-0.099	-0.044	-0.115	-0.083

Table 14: NDCG@5 results (original vs. debias) on 14 datasets for 5 relevance-supervised retrievers.

Dataset (↓)	ANCE		coCondenser		DRAGON		RetroMAE		TAS-B	
	Original	Debias	Original	Debias	Original	Debias	Original	Debias	Original	Debias
MS MARCO	0.590	0.568	0.620	0.621	0.665	0.665	0.626	0.626	0.617	0.617
DL19	0.695	0.706	0.750	0.747	0.767	0.769	0.739	0.743	0.743	0.743
DL20	0.716	0.671	0.750	0.751	0.778	0.779	0.760	0.771	0.737	0.740
TREC-COVID	0.679	0.690	0.707	0.695	0.684	0.681	0.744	0.737	0.644	0.638
NFCorpus	0.301	0.304	0.382	0.381	0.397	0.396	0.373	0.376	0.375	0.381
NQ	0.628	0.626	0.687	0.687	0.737	0.737	0.704	0.704	0.689	0.689
HotpotQA	0.537	0.537	0.640	0.639	0.719	0.719	0.716	0.715	0.674	0.673
FiQA-2018	0.255	0.255	0.244	0.244	0.323	0.322	0.278	0.277	0.257	0.261
Touché-2020	0.487	0.475	0.326	0.333	0.501	0.513	0.444	0.450	0.429	0.415
DBPedia	0.435	0.436	0.525	0.522	0.540	0.540	0.526	0.524	0.518	0.518
SCIDOCS	0.114	0.113	0.124	0.125	0.148	0.146	0.136	0.136	0.138	0.133
FEVER	0.824	0.829	0.785	0.786	0.895	0.894	0.891	0.892	0.858	0.858
Climate-FEVER	0.240	0.245	0.237	0.240	0.290	0.291	0.279	0.283	0.286	0.287
SciFact	0.429	0.427	0.530	0.526	0.599	0.595	0.571	0.574	0.564	0.563
AVG	0.495	0.492	0.522	0.521	0.575	0.575	0.556	0.558	0.537	0.537